Available online at www.sciencedirect.com
SCIENCE DIRECT®
JOURNAL OF CONSTRUCTIONAL STEEL RESEARCH
ELSEVIER Journal of Constructional Steel Research 59 (2003) 951–970
www.elsevier.com/locate/jcsr

Primary creep buckling of steel columns in fire

J.L. Zeng, K.H. Tan, Z.F. Huang *

School of Civil and Environmental Engineering, Nanyang Technological University, 50 Nanyang Avenue, Singapore 639798, Singapore

Received 2 September 2002; received in revised form 20 January 2003; accepted 27 January 2003

Abstract

This paper proposes an analytical method to predict the fire resistance of a pinned-pinned steel column. Traditionally, the column fire resistance is determined through the standard ISO834 fire test. Under this condition, the external load is kept constant while the member temperature rises monotonically. The complicated creep strain, as well as the degradation of steel mechanical properties is taken into account in this approach. The predictions are verified experimentally and numerically. The extensive numerical verifications show that under different external load levels and different slenderness ratios, the proposed analytical method yields accurate predictions. The procedure can be incorporated into spreadsheet application software.

Keywords: Steel column; Fire; Critical temperature; Primary creep

1. Introduction

The structural behaviour of a steel building exposed to fire conditions has long been an interesting, though rather complicated problem for both researchers and engineers. This paper focuses particularly on steel columns. There are various factors that substantially influence the behaviour of a steel column in fire situation, such as the heating scheme, thermal gradient within the column section and boundary restraints [1–3]. Besides, the material properties, such as the elastic modulus and yield stress, continuously deteriorate at a rate depending not only on the fire curve but also on the loading condition. More importantly, it has been demonstrated that creep effect is accelerated at high temperature and this turns out to be rather signifi-

* Corresponding author. Tel.: +65-679-048-51; fax: +65-679-106-76.
E-mail address: czfhuang@ntu.edu.sg (Z.F. Huang).

0143-974X/03/$ - see front matter
doi:10.1016/S0143-974X(03)00027-0

Nomenclature

a,b,c	Material constants in Furumura's model
A	Area of cross section (mm^2)
E_0^{20}	Elastic modulus for instantaneous mechanical strain at 20 °C (MPa)
E_0^T	Elastic modulus for instantaneous mechanical strain at temperature T (MPa)
E_1^T	Tangent modulus beyond yielding for a bi-linear stress-strain curve at temperature T (MPa)
e_T	Relative difference between the predictions of critical temperature (%)
f_y^{20}	Yield strength at ambient temperature (MPa)
f_y^T	Yield strength at elevated temperature T (MPa)
H	Center-to-center distance between two flanges (for I-section, mm)
I	moment of inertia (mm^4)
l	Column length (mm)
m	Primary creep power index
N	Applied axial load (N)
$N_{b,fi,0,Rd}$	design buckling resistance of column at the beginning of fire (N)
P_p	Column plastic strength at room temperature (N)
S	Dimensionless geometry constant
t	Time (h)
T	Temperature (°C)
$TK = T+273.16$	absolute temperature (K)
T_{cr}	Column critical temperature (°C)
w_0	Displacement constant before application of mechanical loading (mm)
$w(x,t)$	At time t, the displacement at location with a distance of x apart from the end support (mm)
W_0	Column initial mid-height lateral displacement (mm)
$W(t)$	Column mid-height lateral displacement at time t (mm)
x	Distance away from the bottom end support (mm)
α	Angle of harmony curve (degree)
β	Material constant in Furumura's model
χ	$= E_0^T/E_1^T$
δ_e	Axial movement of column upper end (mm)
ε	Strain
$W_3(t)$	Strain at the concave and convex flanges, respectively

W	Creep strain pertaining to the concave and convex flanges, respectively
$\varepsilon_1 + \varepsilon_2 = 2\varepsilon_A$	Thermal strain of the concave and convex flanges, respectively
ε_A	Average strain at cross section
ε_{cr}	Creep strain
ε_{ep}	Instantaneous mechanical (i.e. elastic and plastic) strain
ε_{th}	Thermal strain
γ	Material constant in Furumura's model
κ	Curvature
λ	Column slenderness ratio
μ^N	Axial load utilization factor
σ	Stress (MPa)
T	Stress at concave and convex flanges, respectively (MPa)
σ_A	Average stress at cross section (MPa)
σ_E	Euler's buckling stress (MPa)
σ_m	Primary creep material constant
σ_n	Secondary creep material constant

cant for fire safety design [4,5]. Therefore, creep analysis should be considered in the design of structural steel members.

For a given temperature, a typical creep curve of steel material versus time is shown in Fig. 1a, while Fig. 1b shows the corresponding creep rate $d\varepsilon_{cr}/dt$ with

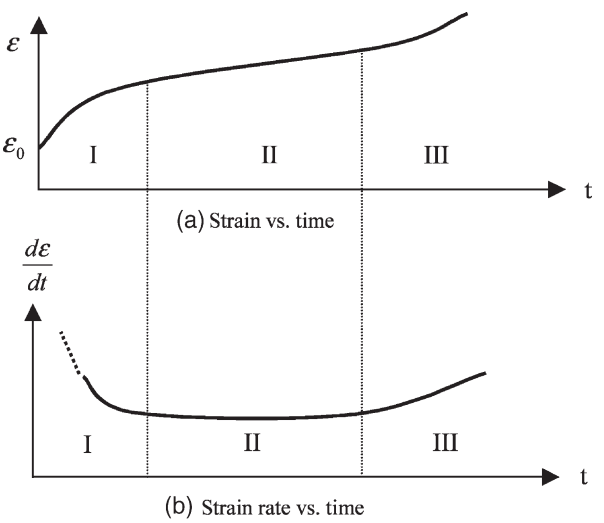

Fig. 1. Strain and strain rate in constant stress and temperature creep test.

time. From Fig. 1b, three distinct periods of creep can be observed, during which time the creep rate is initially decreasing, held constant, and then eventually increasing. These are often associated with periods of primary, secondary, and tertiary creep [6]. In case of building fires, structural steel members mainly experience primary creep due to short fire duration.

To facilitate structural steel design, some existing design codes do provide guidance for fire resistance design, such as CEC [7] and BSI [8], which suggest taking account of creep strain implicitly. However, it should be noted that the creep effect is basically a transient phenomenon, as shown in Fig. 1. Hence, a transient analysis rather than a steady state analysis as assumed by current design codes is more appropriate.

Since the creep properties of material are temperature-dependent, the creep behaviour of a column under varying temperature is different from that under constant ambient temperature. As a result of emerging concern to structural fire safety design during the last two decades, various papers have reported on the short-term creep behaviour, where the temperature increases rapidly. Due to the complexity of the problem, almost all researchers adopt Finite Element Method (FEM) as the analytical tool [4,5,9].

However, this paper presents a semi-analytical approach, which can predict the fire resistance of steel columns reasonably well. The approach is simple and can be carried out in a Microsoft Excel spreadsheet. Besides, it satisfies both the conflicting requirements of structural engineering analysis, that is, the method must be accurate and simple. It must be robust enough to be programmed into spreadsheet application software, such as Microsoft Excel.

2. Research significance

Hult [6] presented a case study of secondary creep buckling of a pinned-pinned steel column made of H section subjected to both constant temperature and axial load. Based on his work, the authors derived some critical failure criteria that govern the primary creep buckling behaviour under increasing temperature, making it possible to predict the fire resistance of pinned-pinned steel columns. The method can be extended to columns of other boundary conditions. This approach is different from prevailing FEM programs, as it can be executed in a spreadsheet, which is available in most personal computers.

2.1. Assumptions

This approach makes the following assumptions:

1. Neither local and nor torsional buckling is considered.
2. Within a column, temperature distribution is uniform across the section and along the member length.

3. Temperature increases rapidly, so that creep buckling occurs within a relatively short time span. Thus, only primary creep is considered.
4. Column is subjected to an initial deflection, due to imperfections arising from manufacturing, handling and/or installation.
5. Boundary restraint effects from surrounding cool structures are not considered.
6. Since this study focuses on steel columns, only uni-axial creep strain is considered.

2.2. Constitutive equations

Based on the spring-dashpot model [6], total primary creep strain consists of three components: instantaneous mechanical strain ε_{ep}, creep strain ε_{cr} and thermal strain ε_{th}, as listed in Eq. (1):

$$\varepsilon = \varepsilon_{ep} + \varepsilon_{cr} + \varepsilon_{th} \tag{1}$$

The primary creep law is written in the following form:

$$\frac{d\varepsilon_{cr}}{dt} = \frac{1}{\tau}\left[\frac{\sigma}{\sigma_m}\right]^m \cdot (\varepsilon_{cr})^{-\mu} \tag{2a}$$

or

$$\frac{d}{dt}(\varepsilon_{cr})^{1+\mu} = \frac{1+\mu}{\tau}\left[\frac{\sigma}{\sigma_m}\right]^m \tag{2b}$$

where σ_m, m and μ are material parameters and are functions of temperature T; τ is a fixed standard time unit. The term μ is sometimes called strain-hardening exponent, and $\mu \geq 0$. This creep law includes the limiting case, that is, when $\mu = 0$, Eq. (2) is reduced to the famous secondary creep equation—the Bailey–Norton law, which forms the backbone of secondary creep analysis:

$$\frac{d\varepsilon_{cr}}{dt} = \frac{1}{\tau}\left|\frac{\sigma}{\sigma_n}\right|^n \mathrm{sgn}\sigma \tag{3}$$

where signum function is defined by

$$\mathrm{sgn}\sigma = \begin{cases} -1 & \sigma < 0: \quad \textit{tensile} \\ 0 & \sigma = 0 \\ +1 & \sigma > 0: \quad \textit{compressive} \end{cases}$$

The experimental results reveal that, in the region of primary creep strain, the compressive-creep curve is identical to the tensile-creep curve. Thus, the primary creep law, established for tensile stresses, may also be used for compressive stresses in the following form:

$$\frac{d}{dt}(\varepsilon_{cr})^{1+\mu} = \frac{1+\mu}{\tau}\left|\frac{\sigma}{\sigma_m}\right|^m \mathrm{sgn}\sigma \tag{4}$$

In case of primary creep buckling under fire conditions, where the temperature increases rapidly, the material yield stress f_y^T keeps reducing until at a certain time, it is smaller than the applied stress σ. The instantaneous plastic strain is incorporated through a bilinear $\sigma-\varepsilon$ curve [4] (see Fig. 2):

$$\varepsilon_{ep} = \underbrace{\frac{\sigma}{E_0^T}}_{\text{elastic}} + \underbrace{(\sigma - f_y^T)\left(\frac{1}{E_1^T} - \frac{1}{E_0^T}\right) u(\sigma - f_y^T)}_{\text{plastic}} \tag{5}$$

where E_0^T is elastic modulus and E_1^T is plastic stress-strain modulus at elevated temperature T after the yield strength f_y^T is exceeded (Fig. 2). The step function $u(\sigma - f_y^T)$ is defined as:

$$u(\sigma - f_y^T) = \begin{cases} 0 & \sigma < f_y^T \\ 1 & \sigma > f_y^T \end{cases} \tag{6}$$

On the other hand, the thermal strain ε_{th} can be calculated as a function of temperature. In the current work, thermal expansion (tension) is defined as negative strain. For instance, ε_{th} of steel grade SM50 is characterized by [4]:

$$\varepsilon_{th} = -(5.04 \times 10^{-9} T^2 + 1.13 \times 10^{-5} T) \tag{7}$$

where T is in °C.

Clearly, Eqs (1), (4), (5) and (7) form the constitutive equations of primary creep buckling problem.

2.3. Geometry of steel columns

Most steel columns consist of I-section because of its relatively larger second moment of area to resist bending. The overall buckling failure about the major axis can be substantially simplified with the following section transformation, as shown

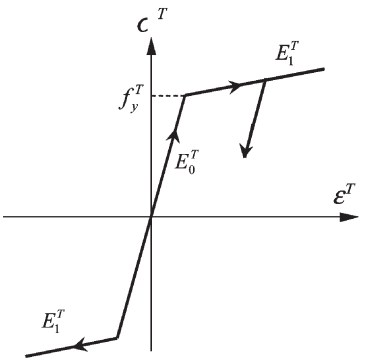

Fig. 2. Steel stress–strain relationship at elevated temperature.

in Fig. 3 [10,11]. After the transformation, the stress distribution across the section is statically determinate, but stress distribution along the member length remains unknown.

It is assumed that the heated column deforms in sinusoidal curve, and that the profile will remain essentially sinusoidal throughout the creep buckling process. Hence, from Fig. 4, the deflection curve is given by

$$w(x,t) = W(t)\sin\frac{\pi x}{l} \tag{8}$$

where the distance x along column axis and time t are uncoupled, and $W(x)$ represents the initial deflection amplitude at mid-height. If the initial crookedness of the column is not a half sine wave but some other general shapes, the deflection curve can be expressed as a Fourier sine series:

$$w(x,t) = W_1(t)\sin\frac{\pi x}{l} + W_2(t)\sin\frac{2\pi x}{l} + W_3(t)\sin\frac{3\pi x}{l} + \cdots \tag{9}$$

The analysis of a steel column with a general shape is rather complex. However, Kempner and Patel [12] have proved that the inclusion of a second or third harmonic in the initial deformation curve does not essentially change the first-harmonic character of creep deformation, except when the amplitudes of both the second and higher harmonics of initial crookedness are very large, that is, $W_2(t)$ and $W_3(t)$ in Eq. (9). Thus, the analysis of column creep buckling based on one single harmonic deformation curve is sufficient to produce a reasonable approximation.

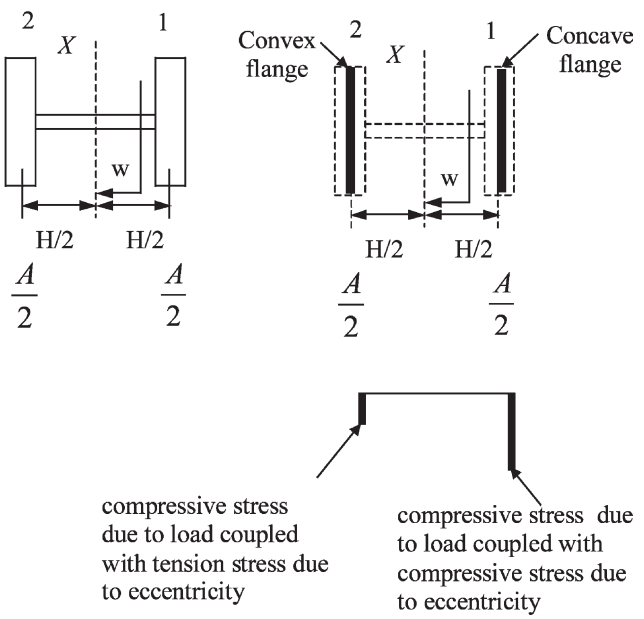

Fig. 3. A real I-section vs. an idealized I-section.

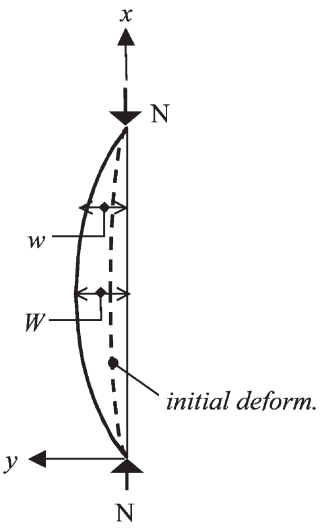

Fig. 4. General deformation curve for a pinned-pinned column.

2.4. Primary creep buckling under varying temperature

A case study is presented here which consists of a pinned-pinned steel column subjected to a constant axial force P and elevated temperature T (Fig. 4). The cross-section is shown in Fig. 3, whereby the section properties of half the web and flange congregate along the solid line at $H/2$ from the centroid. Adopting positive sign convention for compressive stress, the equilibrium equations for force P and secondary moment $P\ w$ read as:

$$\frac{\sigma_1 A}{2} + \frac{\sigma_2 A}{2} = \sigma_A A = P \tag{10a}$$

$$\frac{\sigma_1 AH}{4} - \frac{\sigma_2 AH}{4} = P\ w(x,t) \tag{10b}$$

where $\sigma_A = P/A$ is the mean axial compressive stress in column;

$$w(x,t) = W(t)\sin\alpha, \alpha = \pi\ x/l \tag{11}$$

$w(x,t)$ is the deflection at any point along the column axis and at time t; W is the mid-height lateral deflection.

On the other hand, the general curvature equation is given as:

$$\frac{\dfrac{\partial^2 w}{\partial x^2}}{\left[1 + \left(\dfrac{\partial w}{\partial x}\right)^2\right]^{1.5}} = \kappa(\text{curvature}). \tag{12}$$

Applying small deflection theory, if

$$\frac{\partial w}{\partial x} = \frac{\pi}{l} W \cos\frac{\pi x}{l} \leq 0.2 \tag{13}$$

Eq. (12) can therefore be simplified to

$$\frac{\partial^2 w}{\partial x^2} = \kappa \tag{14}$$

At the column bottom end ($x = 0$ in Fig. 4), Eq. (13) is equivalent to

$$\frac{W}{l} \leq 0.0637 \tag{15}$$

Thus, within the small deformation scope, the following mechanical equations can be derived:

$$\begin{aligned} &\varepsilon_1 + \varepsilon_2 = 2\varepsilon_A \\ &\varepsilon_1 - \varepsilon_2 = -H\left(\frac{\partial^2 w}{\partial x^2} - \frac{\partial^2 w_0}{\partial x^2}\right) = S(\Delta - \Delta_0)\sin\alpha \end{aligned} \tag{16}$$

where ε_A denotes the mean axial compressive strain in column;

$$S = \frac{(\pi H)^2}{2 I^2}$$

$$\Delta = \frac{2W}{H}, \Delta_0 = \frac{2W_0}{H}$$

W_0 is the initial mid-height lateral deflection.

In the concave flange (Fig. 3), the stress σ_1 increases monotonically during deformation. Applying Eqs (4), (5) and (7) into Eq. (1), one obtains

$$\left(\frac{d\varepsilon_1}{dt}\right) = \underbrace{\frac{1}{E_0^T}\frac{d\sigma_1}{dt} - \frac{\sigma_1}{(E_0^T)^2}\frac{dE_0^T}{dt}}_{\text{elastic}} + \underbrace{\frac{1}{\tau}\left(\frac{\sigma_1}{\sigma_m}\right)^m (\varepsilon_{1,cr})^{-\mu}}_{\text{creep}} + \underbrace{\frac{d\varepsilon_{1,th}}{dt}}_{\text{thermal}} + \underbrace{\frac{d\varepsilon_{1,p}}{dt}}_{\text{plastic}} \tag{17}$$

where

$$\varepsilon_{1,cr} = \varepsilon_A + \frac{S}{2}(\Delta - \Delta_0) - \frac{\sigma_A}{E_0^{20}}(1 + \Delta)$$

$$\frac{d\varepsilon_{1,p}}{dt} = \left[\frac{1}{E_0^T}\frac{d(\sigma_1 - f_y^T)}{dt} - \frac{(\sigma_1 - f_y^T)}{(E_0^T)^2}\frac{dE_0^T}{dt}\right](\chi - 1)\, u(\sigma_1 - f_y^T)$$

$$\chi = E_0^T / E_1^T$$

On the other hand, the stress in the convex flange decreases. In this case, the plastic strain term is deleted since the unloading strain curve is parallel to the initial elastic strain curve (Fig. 2). Therefore, it leads to

$$\left(\frac{d\varepsilon_2}{dt}\right) = \underbrace{\frac{1}{E_0^T}\frac{d\sigma_2}{dt} - \frac{\sigma_2}{(E_0^T)^2}\frac{dE_0^T}{dt}}_{\text{elastic}} + \underbrace{\frac{1}{\tau}\left|\frac{\sigma_2}{\sigma_m}\right|^m (\varepsilon_{2,cr})^{-\mu}\text{sgn}\sigma_2}_{\text{creep}} + \underbrace{\frac{d\varepsilon_{2,th}}{dt}}_{\text{thermal}} \tag{18}$$

where

$$\varepsilon_{2,cr} = \varepsilon_A - \frac{S}{2}(\Delta - \Delta_0) - \frac{\sigma_A}{E_0^{20}}(1 + \Delta)$$

From Eqs (16–18), two simultaneous differential equations can be obtained by considering the summation and subtraction of differential strain rates of the concave and convex flanges:

$$\frac{d(\varepsilon_1 + \varepsilon_2)}{dt} = 2\frac{d\varepsilon_A}{dt} \tag{19a}$$

and

$$\frac{d(\varepsilon_1 - \varepsilon_2)}{dt} = S\sin\alpha\cdot\frac{d\Delta}{dt} \tag{19b}$$

Under the assumption of plane-cross-section-remains-plane after deformation, Eq. (19) is true for any cross-section. Eq. (19a) gives the rate of increase of mean axial compressive strain ε_A, whereas Eq. (19b) calculates the rate of increase of non-dimensional column mid-height deformation ($\Delta = 2W/H$). At column mid-height ($\alpha = \pi/2$), Eq. (19) leads to

$$\frac{d\varepsilon_A}{dt} = -\frac{\sigma_A}{(E_0^T)^2}\frac{dE_0^T}{dt} + \frac{1}{2\tau}\left(\frac{\sigma_A}{\sigma_m}\right)^m\left[\frac{(1 + \Delta)^m}{(\varepsilon_{1,\,cr})^\mu} + \frac{|1-\Delta|^m\text{sgn}(1-\Delta)}{|\varepsilon_{2,\,cr}|^\mu}\right] + R_1 + \frac{d\varepsilon_{1,th}}{dt} \tag{20}$$

and

$$\frac{d\Delta}{dt}\left(\frac{\sigma_E - \sigma_A}{E_0^T}\right) = \frac{-\sigma_A}{(E_0^T)^2}\Delta\frac{dE_0^T}{dt} + \frac{1}{2\tau}\left(\frac{\sigma_A}{\sigma_m}\right)^m\left[\frac{(1 + \Delta)^m}{(\varepsilon_{1,\,cr})^\mu} - \frac{|1-\Delta|^m\text{sgn}(1-\Delta)}{|\varepsilon_{2,\,cr}|^\mu}\right] + R_1 \tag{21}$$

where

$$R_1 = \left\{\frac{\sigma_A d\Delta}{E_0^T dt} - \frac{1}{E_0^T}\frac{df_y^T}{dt} - \frac{[\sigma_A(1 + \Delta) - f_y^T]dE_0^T}{(E_0^T)^2\quad dt}\right\}\frac{(\chi-1)}{2}u[\sigma_A(1 + \Delta) - f_y^T]$$

$\sigma_E = \dfrac{P_E}{A}$ denotes Euler buckling stress;

$P_E = \dfrac{\pi^2 E_0^T I}{l^2}$ denotes Euler buckling load for a pinned − pinned column.

Here, σ_A denotes the mean axial compressive stress (cf. Eq. (11)). Thermal strain ε_{th} is purely a function of temperature, which is itself a function of time, so that the derivative thermal strain with respect to time $\frac{d\varepsilon_{th}}{dt}$ in Eq. (20) can be obtained by chain rule, provided the temperature-time relation $T-t$ is known. Thus, Eqs (20) and (21) are the simultaneous governing equations for numerical approximation, which can be expressed in the form of two functions f and g

$$\frac{d\varepsilon_A}{dt} = f(\varepsilon_A, \Delta, t, \frac{d\Delta}{dt}) \tag{22a}$$

and

$$\frac{d\Delta}{dt} = g(\varepsilon_A, \Delta, t) \tag{22b}$$

Eq. (22a) can be rearranged into

$$\frac{d\varepsilon_A}{dt} = \varphi(\varepsilon_A, \Delta, t) \tag{23}$$

The buckling failure criterion is defined as the critical creep-buckling time, at which $d\Delta/dt$ (Eq. (21)) tends to infinity at mid-height. In this context, it is clear from Eq. (21) that a steel column fails due to

- Overall primary creep buckling when $\sigma_A \geq \sigma_E$, or
- when $\sigma_A < \sigma_E$,

$$\frac{d\Delta}{dt} = \infty \tag{24}$$

Obviously, the condition $\sigma_A \geq \sigma_E$ implies that the external load N is equal to or greater than the column Euler load P_E at room temperature. That is, the column buckles instantly at the beginning of heating.

2.5. Proposed method algorithm and program PMCB

Based on the derived governing equations and failure criteria, an algorithm for numerical approximation is delineated in Fig. 5. It is noteworthy that in the numerical approximation, a column is assumed to fail when

$$W = \Delta H \geq 0.0637\, l \tag{25}$$

A Visual Basic program PMCB (PriMary Creep Buckling), which is resident in Excel spreadsheet, has been developed for the fire resistance analysis of steel columns in fire conditions.

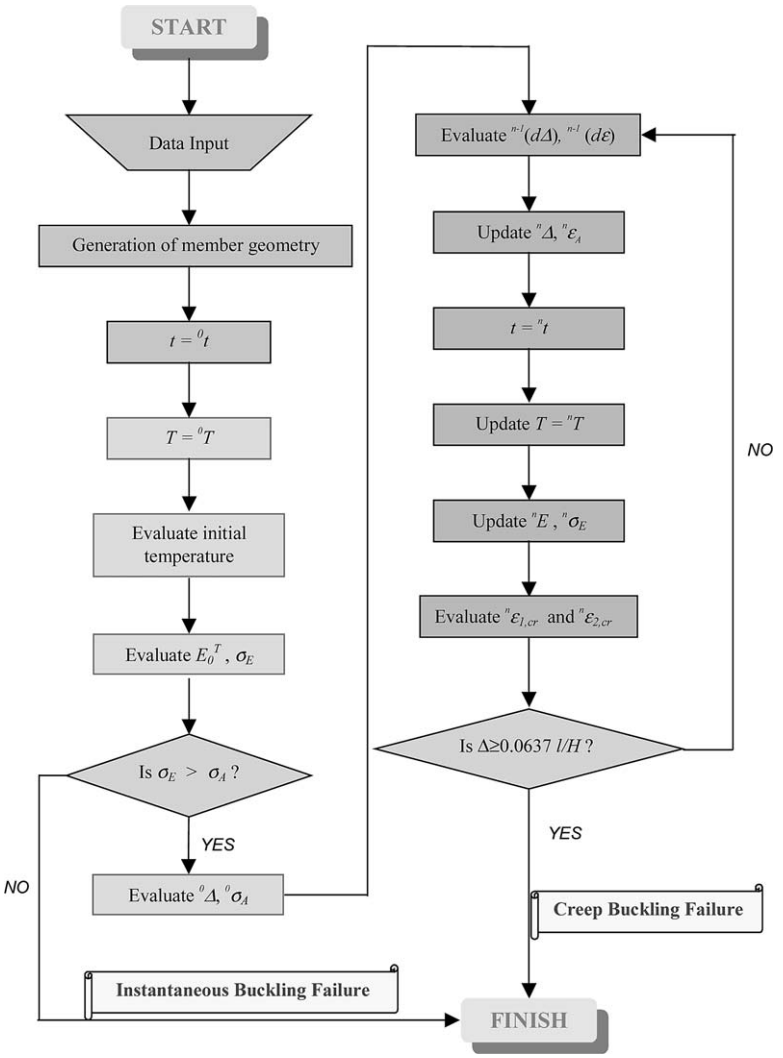

Fig. 5. Applied algorithm of program PMCB.

2.5.1. *Verification*

In the following, the proposed approach is verified against experimental and numerical analyses. A visco-elasto-plastic finite element program FEMFAN5 is used in the numerical verification. For comparison purpose, it should be noted that the failure criteria of FEMFAN have been adjusted to match those of PMCB. This adjustment will not affect the predictions of FEMFAN on the critical temperature of columns under study, since they experience only small deformations upon failure. The maximum difference in term of column critical temperature caused by this adjustment is less than 0.5 °C.

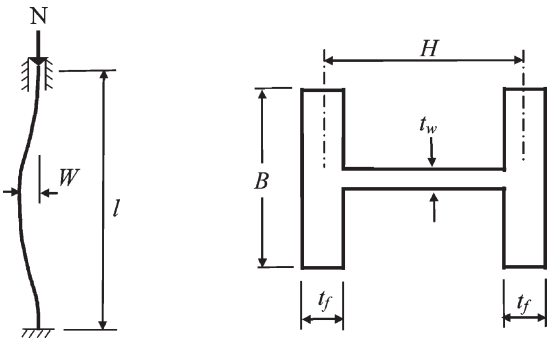

Fig. 6. Tested members' geometry.

Table 1
Values of tested columns parameters [13]

No. (1)	Cross-section (2)	l [mm] (3)	H[mm] (4)	B [mm] (5)	t_f [mm] (6)	t_w [mm] (7)	A [m^2] (8)	N [kN] (9)
1	W10 × 60	3760	242.5	257	17.5	11.1	0.01142	1760
2	W10 × 49	3760	239.7	254	14.3	7.9	0.00929	1424

2.6. Experimental Verification—1

Ginda and Slowronski [9] proposed a computational model to predict the load capacity of a thin-walled steel column in fire. Their model and the proposed approach here were verified against two fire tests of axially-loaded steel columns [13]. The columns were made from standard American structural steel ASTM-A36 and American profiles (W10 × 60, W10 × 49). The axial compressive force N was held constant during the fire tests. A constant temperature rise of 4 °C/min was maintained. Fig. 6 shows a typical column section, while Table 1 and Table 2, respectively, contain section geometry and the chemical composition of Japanese steel SM50 and American steel ASTM A36. The steel properties employed in this case study are quoted from Ref. [4], since the chemical composition of SM50 is almost identical to ASTM

Table 2
Comparison of steel SM50 with ASTM A36

Steel type (1)	Carbon [%] (2)	Manganese [%] (3)	Silicon [%] (4)	Tensile strength (MPa) (5)
SM50	<0.20	<1.6	<0.55	500
ASTM A36	<0.25	<1.2	<0.40	500
S235	<0.20	<1.4	<0.50	340–500

A36 (see Table 2). Since both column ends are rotationally restrained, only one-half of column length is analysed by PMCB.

Lie and Macaulay [13] relied on the longitudinal displacement of column upper end δ_e to quantify two failure criteria. The first criterion assumed that the critical temperature of a column is reached when the value of δ_e reaches maximum (i.e. the column top end increases to its maximum position). The second criterion was based on large intensification of changes and loss of ability to measure δ_e. The respective values of measured critical temperature T_{cr} corresponding to the first or second criterion, are indicated before and after the slash in column (3) of Table 3. The terms T_{cr}^{Test} and T_{cr}^{PMCB} in Table 3 represent the critical temperature obtained by test and program PMCB, respectively.

The thermal strain ε_{th} is computed from Eq. (7).

The steel elastic modulus E_0^T at elevated temperature can be calculated as:

$$E_0^T = (-8.75 \times 10^{-7}T^2 - 3.87 \times 10^{-4}T + 1.008)\, E_0^{20} \tag{26}$$

in which E_0^{20} is elastic modulus at ambient temperature and T is in °C.

The original expression for creep deformation in Furumura's work is stated as:

$$\frac{d\varepsilon_{cr}}{dt} = 10^{\left(c-\frac{a}{2.3T}\right)\frac{1}{\gamma}} \cdot \left(\frac{2.37 \times |\sigma|}{3.4}\right)^{\left(\frac{b}{2.3T}+\beta\right)\frac{1}{\gamma}} \cdot \gamma\left(\frac{\gamma-1}{\gamma}\right) \cdot (\varepsilon_{cr})^{\frac{\gamma-1}{\gamma}} \cdot \mathrm{sgn}\sigma \tag{27}$$

Rearranging Eq. (27) into the format of Eq. (3), one obtains

$$\frac{d\varepsilon_{cr}}{dt} = \frac{1}{\tau}\left[\frac{\sigma}{\sigma_m}\right]^m \cdot (\varepsilon_{cr})^{-\mu} \tag{28}$$

where

$$\begin{aligned} \frac{1}{\tau} &= 10^{\left(c-\frac{a}{2.3TK}\right)\frac{1}{\gamma}} \cdot \gamma\left(\frac{\gamma-1}{\gamma}\right) \\ \sigma_m &= \frac{3.4}{2.37} \\ m &= \left(\frac{b}{2.3T} + \beta\right)\frac{1}{\gamma} \\ \mu &= \frac{1-\gamma}{\gamma} \end{aligned} \tag{29}$$

Table 3
Comparison of test results with analytical results—1 (°C)

No. (1)	Cross-section(2)	T_{cr}^{Test}(3)	T_{cr}^{PMCB}(4)	(Ginda and Skowronski [9]) (5)
1	W10 × 60	510/575	532	473
2	W10 × 49	530/630	533	461

In Eqs (27–29), constants $a = 45\ 000$, $b = 19\ 000$, $c = 20.53$, $\gamma = 0.35$, $\beta = -7.25$; temperature TK is in Kelvin, time t in minutes, stress σ in kg/mm^2 (=9.81 MPa) and creep strain ε_{cr} in percentage (%).

The test results, numerical predictions of proposed method and Ginda and Slowronski [9] are included in Table 3, which shows that the simple semi-analytical approach (column (4)) yielded good agreement. The numerical results in the last column are based on a Finite Difference method [9].

The numerical approximation is executed at 0.1 °C interval. The critical buckling temperatures are shown in column (4) of Table 3. The differences between the predictions of proposed approach and fire tests can be attributed to the following beneficial factors. For example, the actual ultimate strength and elastic modulus of steel material are greater than those adopted by our approach. Moreover, during heating, column ends normally attain lower temperatures compared to mid-height section.

2.7. Experimental verification—2

Franssen et al. [14] reported series of standard fire resistance tests on I-section steel columns under small load eccentricities. The tests were conducted at the Technische Universität Braunschweig, Germany. This paper only presents the experimental work of pin-rollered columns subjected to very small load eccentricities. They generally failed about their strong axis. Table 4 shows the information of those 13 columns, as well as the critical temperatures predicted by both the test and our approach. The steel grade is S235, which is equivalent to SM50 (Table 2). Thus, PMCB uses stress–strain model (Eq. (26)) of SM50 for the analysis. The structural temperature is assumed to rise at 5 °C/min.

Table 4
Comparison of test results with analytical results—2

No. (1)	Cross-section (2)	l [mm] (3)	λ (4)	f_y [MPa](5)	e [mm] (6)	N [kN] (7)	N/f_yA (8)	T_{cr}^{test}[°C] (9)	T_{cr}^{PMCB}[°C] (10)
1	HEB 120	3800	75.4	257	0	317.8	0.364	560	515
2	HEM 220	3800	38.4	269	12	1268	0.316	600	548
3	HEB 220	3800	40.3	261	12	767.1	0.323	590	543
4	HEA 220	3800	41.4	309	12	783.8	0.394	560	508
5	HEM 220	4800	48.5	269	14	695	0.173	650	586
6	HEB 120	4800	95.2	257	12	105	0.120	685	581
7	HEB 180	3860	50.4	267	0	891	0.511	475	496
8	HEB 220	3700	39.2	269	12	1489	0.608	335	483
9	HEB 220	3700	39.2	249.5	12	1628	0.717	230	476
10	HEB 220	3700	39.2	263.3	12	1136	0.474	478	510
11	HEB 160	4700	69.3	261.8	12	755	0.532	232	489
12	HEB 160	4700	69.3	248.6	12	650	0.482	290	486
13	HEB 160	4700	69.3	259.2	12	590	0.420	412	496

The comparison of critical temperatures is also shown in Fig. 7. Obviously, there exist significant differences between the test results and PMCB predictions for four columns, although for the remaining columns, two predictions agree quite well. The large differences can be due to the uneven temperature distribution across or along the columns, which generated significant thermal bowing. Table 4 shows that these four columns are all subjected to relatively high load levels with ratio N/f_yA ranging from 0.482–0.717. This means that these four columns are very sensitive to $P-\Delta$ effect, which can be exaggerated by the potential thermal bowing.

Due to the diversity nature of fire tests, it is fairer to appraise the accuracy of the PMCB by extensively comparing the predictions of this approach with those of finite element analysis.

2.8. Numerical verification

In this verification, steel columns are made of ASTM-A36 and their section is W10 × 60. Four groups of steel columns with different slenderness ratios λ are investigated, namely, λ = 20, 50, 100 and 150. All columns are pin-rolled and have an initial sinusoidal lateral deflection with $W_0/l = 1/1000$. With regard to the external axial load N, the axial load utilization factor [7] μ^N, which is defined as a ratio of external axial load N to column buckling resistance $N_{b,fi,0,Rd}$ at the beginning of heating (see Eq. (30)), is adopted

$$\mu^N = \frac{N}{N_{b,fi,0,Rd}} \tag{30}$$

For the calculation of $N_{b,fi,0,Rd}$, please refer to CEC [7]. In this paper, μ^N takes on 0.10–0.70 at a step of 0.10. For columns of λ = 20, 50, 100 and 150, their respective $N_{b,fi,0,Rd}$ are equal to $0.817P_p$, $0.682P_p$, $0.368P_p$ and $0.190P_p$ (here, $P_p = f_y^{20}A$ is the column plastic strength at room temperature). Only bending action about the major axis is investigated. The column temperature rises at 4 °C per min, and only uniform

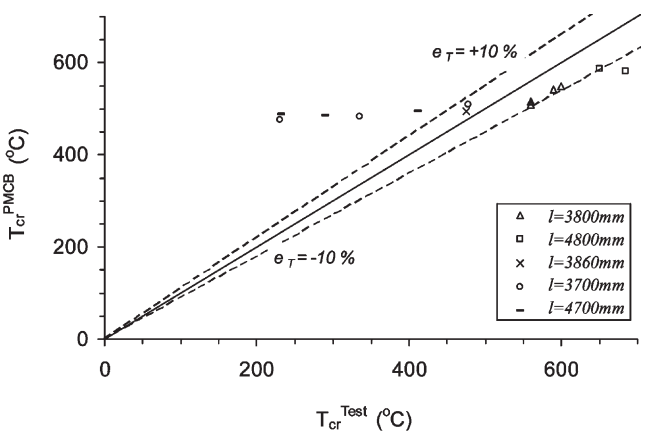

Fig. 7. Column critical temperatures predicted by PMCB and experiments.

temperature distribution along the column length and across the section is considered. A total of four (different λ) by seven (different μ^N) = 28 columns is under investigation.

Critical temperatures T_{cr} predicted by the analytical approach and finite element program FEMFAN are presented in Fig. 8, in which T_{cr}^{PMCB} and T_{cr}^{FEMFAN} represent predictions obtained by PMCB and FEMFAN, respectively. It should be noted that the program FEMFAN has small-strain–large-deformation capability. However, for consistency in comparison, the large deformation capability is switched off. Besides, each column is divided into four elements of equal length.

For comparison purpose, relative difference index e_T is defined as

$$e_T = \frac{T_{cr}^{PMCB} - T_{cr}^{FEMFAN}}{T_{cr}^{FEMFAN}} \tag{31}$$

It should be noted that in Fig. 8, for each slenderness ratio group, the greater the load utilization factor μ^N, the lower is the critical temperature. Fig. 8 clearly reveals that T_{cr}^{PMCB} evenly distributes, mostly within the ±5% scatter band. Fig. 8 also shows that the proposed analytical method tends to overestimate the column critical temperature as column becomes slenderer. This trend becomes significant under a high utilization factor. It can be attributed to the following two reasons:

- Current analytical approach slightly underestimates $P-\delta$ effect. It should be noted that PMCB applies incremental solution scheme under a particular time step, while FEMFAN uses iteration scheme. In other words, PMCB tends to give a lower bound estimate of lateral deflection.
- PMCB assumes that the entire column deform in one sine curve, while FEMFAN adopts cubic shape function to approximate the lateral deformation. The latter approximates the deformed column more closely.

Besides, the column mid-height deflection W predicted by two methods for differ-

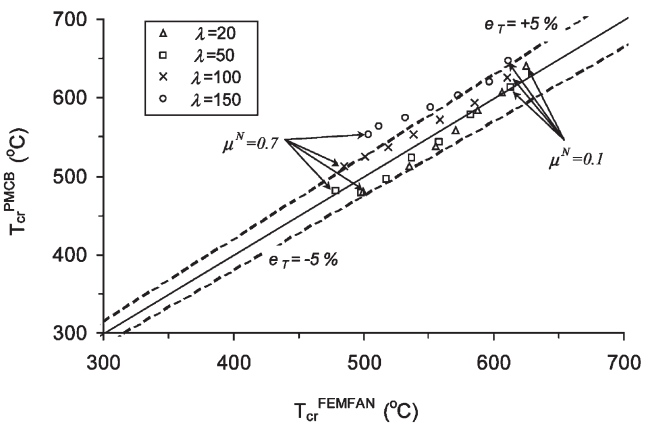

Fig. 8. Column critical temperatures predicted by PMCB and FEMFAN.

ent slenderness ratios under $\mu^N = 0.6$ is shown in Fig. 9. The continuous curves represent PMCB predictions, while the dashed ones represent FEMFAN solutions. Clearly, at the early heating stage when $P-\delta$ effect is not significant, the two methods agree very well. However, towards the end of heating, PMCB tends to predict less deflection than FEMFAN, especially for very slender columns (λ = 150).

In general, Fig. 8 reveals that within the practical design range of μ^N (i.e. 0.3–0.7) and λ (20–100), two approaches agree well in terms of their predictions.

2.9. Effects of initial deflection

The effect of initial lateral deflection on T_{cr} is also examined using PMCB. Two series of columns with λ = 20 and 100, which are extracted from the last section Numerical verification, are investigated. These columns are subjected to four load utilization factors (μ^N = 0.1, 0.3, 0.5 and 0.7), and each column is assigned with four relative initial deflection values ($W_0/l = 1/1000$, $1/500$, $1/100$ and $1/50$). These values have covered the practical range. Critical temperatures are plotted in Fig. 10 and Fig. 11 for λ = 20 and 100 columns, respectively.

Figs 10 and 11 highlight the following points in column failure under fire conditions:

- Small amount of initial imperfection does not affect the column critical temperature substantially, although it initiates creep deformation and buckling process. The column critical temperature tends to be constant when $W_0/l \leq 1/100$, which is representative of the majority of columns encountered in practice.
- When W_0/l is greater than $1/100$, column critical temperature is noticeably reduced by the initial deflection under a high load level ($\mu^N \geq 0.5$).

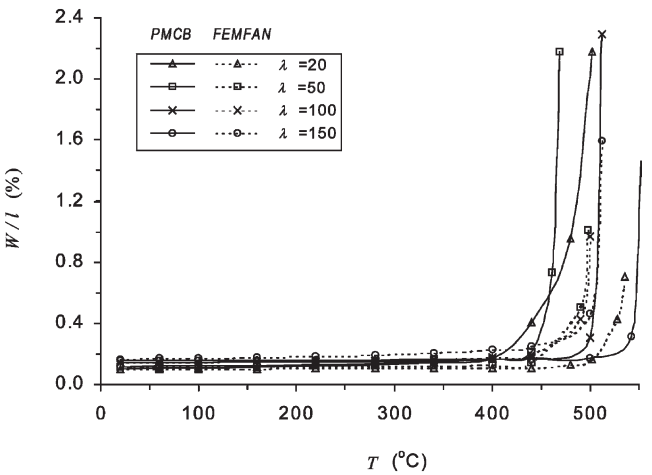

Fig. 9. Column mid-span deflections predicted by PMCB and FEMFAN.

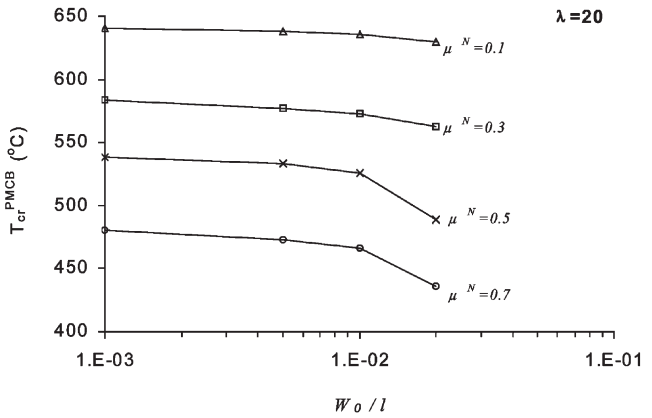

Fig. 10. Effect of Initial Deflection on $\lambda = 20$ column critical temperature by PMCB.

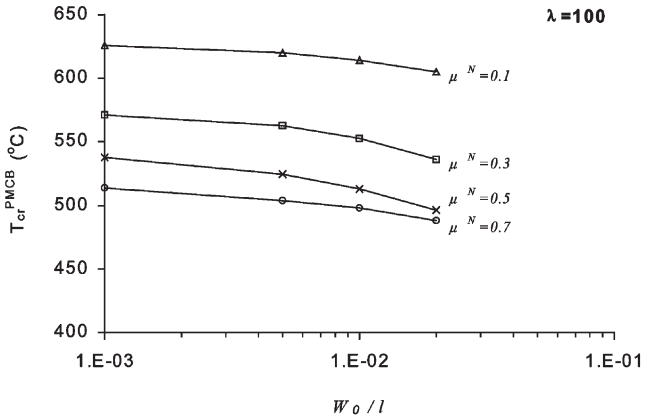

Fig. 11. Effect of initial deflection on $\lambda = 100$ column critical temperature by PMCB.

The numerical study shows that the failure of steel columns is the consequence of various factors. Again, it should be noted that these observations can only be applied to a pinned-pinned steel column subjected to constant axial load and monotonically rising temperature. Further study is required to understand the behaviour of a steel column within a building, which experiences thermal restraints from surrounding cool structure and is subjected to uneven temperature distribution.

3. Conclusion

This study provides some insight into the primary creep buckling of steel columns.

In the present work, a set of critical failure criteria has been developed to investigate the primary creep buckling of a steel column with H section, subjected to con-

stant compressive loading and fully exposed to rapidly elevated temperature. Equilibrium condition and material constitutive equations are utilized to solve this special case. The initial elastic-plastic strain, thermal strain, and creep strain are taken into account.

A close agreement with both the test results and finite element analysis (by FEMFAN) shows that the proposed approach can be utilized as an analytical tool to ascertain the critical column buckling temperature. It not only yields reasonably accurate results by explicitly incorporating the creep behaviour, but at the same time, it is relatively easy to program.

Acknowledgements

The first author likes to express his gratitude to Assoc. Prof. Ng Heong Wah (School of MPE, NTU), for his help rendered in the searching of creep data for steel material.

References

[1] Bailey CG, Moore DB, Lennon T. The structural behaviour of steel columns during a compartment fire in a multi-storey braced steel-frame. J Construct Steel Res 1999;52:137–57.
[2] El-Rimawi JA, Burgess IW, Plank RJ. Studies of the behaviour of steel subframes with semi-rigid connection in fire. J Construct Steel Res 1999;49:83–98.
[3] Huang ZF, Tan KH, Ting SK. Axial restraint effects on the behaviour of steel columns in fire. In: The Eighth East Asian–Pacific Conference on Structural Engineering and Construction (EASEC-8), 5–7 December, Singapore. 2001.
[4] Furumura F, Shinohara Y. Inelastic behaviour of protected steel beams and frames in fire. In: Report of the Research Laboratory of Engineering Materials, No.3. Japan: Tokyo Institute of Technology; 1978. p. 1–14.
[5] Tan KH, Ting SK, Huang ZF. Visco-elasto-plastic analysis of steel frames in fire. J Struct Engng ASCE 2002;128(1):105–14.
[6] Hult JAH. Creep in Engineering Structures. USA: Blaisdell Publishing Company, 1966.
[7] Commission of European Communities. Design of Steel Structures: Part 1.2. General Rules. Structural Fire Design (EC3-Pt. 1.2), Eurocode 3, Brussels, Belgium, 1995.
[8] British Standard Institution. Code of Practice for Fire Resistant Design: Structural Use of Steelwork in Building. Part 8, BS5950, London, UK, 1990.
[9] Ginda G, Skowroński W. Elastic-plastic creep behaviour and load capacity of steel columns during fire. J Construct Steel Res 1998;46:1–3 paper No. 343.
[10] Hoff NJ. Buckling at high temperature. J Roy Aeronaut Soc 1957;61:563.
[11] Hoff NJ. Structure and materials for finite lifetime. Advances in Aeronaut Sciences 1959;2.
[12] Kempner J, Patel SA. Effect of higher-harmonic deflection components on the creep buckling of columns. Aeronautical Quarterly 1957;8.
[13] Lie TT, Macaulay BA. Evaluation of the Fire Resistance of Protected Steel Columns. Ottawa, Canada: NRC, Institute for Research in Construction, 1989 Internal Report No.583, (Coded by Ref. [9]).
[14] Franssen JM, Schleich JB, Cajot LG, Azpiazu W. A simple model for the fire resistance of axially loaded members—Comparison with experimental results. J Construct Steel Res 1996;37:175–204.